RSC Advances

PAPER

View Article Online
View Journal | View Issue

Cite this: *RSC Adv.*, 2025, **15**, 5889

Charge transition levels and stability of Ni- and Ir-doped β-Ga_2O_3: a comprehensive hybrid functional study

Quoc Duy Ho,[a] K. Dien Vo,[bc] Nguyen Thanh Tien,[d] Huynh Anh Huy,[e] Duc-Quang Hoang[fg] and Duy Khanh Nguyen *[hi]

In this study, the optimized hybrid functional HSE(0.26,0.0) is employed to investigate the incorporation of nickel (Ni) and iridium (Ir) dopants in β-Ga_2O_3. The formation energies and charge transition levels of Ni and Ir at gallium sites are calculated. The results show that Ni prefers substitution at the octahedral (Ga_2) site, with a formation energy approximately 1 eV lower than at the tetrahedral (Ga_1) site. Ni at the Ga_2 site (Ni_{Ga_2}) exhibits both donor and acceptor behaviors, with charge transition levels at (+1/0) 1.0 eV and (0/−1) 2.24 eV above the VBM, respectively. Ir similarly favors the octahedral site, displaying donor behaviors with charge transition levels at (+2/+1) 1.04 eV and (+1/0) 3.15 eV above the VBM. Our computational findings for the charge transition levels of Ni and Ir ions are in good agreement with recent experimental measurements, and they explain the correlation between Ni^{3+} and Ir^{4+} ion concentrations observed in electron paramagnetic resonance studies. Additionally, the calculated vertical transitions at 2.56 eV and 4.25 eV for Ni_{Ga_2}, and at 2.91 eV and 4.62 eV for Ir_{Ga_2}, below the conduction band minimum, are in good agreement with optical absorption results, confirming the presence of Ni and Ir substitutions at the Ga_2 site in β-Ga_2O_3. These computational results provide a detailed understanding of the behavior of Ni- and Ir-doped β-Ga_2O_3, highlighting the potential applications of Ni- and Ir-doped β-Ga_2O_3 for optoelectronic devices.

Received 25th December 2024
Accepted 6th February 2025

DOI: 10.1039/d4ra09002k

rsc.li/rsc-advances

1. Introduction

The monoclinic phase of gallium oxide (β-Ga_2O_3), which is the most thermodynamically stable phase of Ga_2O_3, has a large band gap of approximately 5 eV.[1,2] In recent years, β-Ga_2O_3 has received a lot of attention and is considered a new competitor to 4H–SiC and GaN materials. In addition to its high thermal and chemical stability, the wide to ultra-wide band gap of β-Ga_2O_3, resulting in a high breakdown field of around 8 MV cm^{-1}, makes it a potential candidate for applications in high power electronics.[3,4] The availability of high-quality single crystals and thin films of β-Ga_2O_3 holds significant promise for applications in gas sensors,[5,6] electroluminescent devices,[7,8] and photocatalysis.[9–11]

Unintentional dopants such as Si and H are often present in β-Ga_2O_3 crystals, leading to a moderate n-type doping concentration of around mid-10^{17} cm^{-3}.[12–14] Additionally, Sn, Ge, and Nb impurities are also used to create n-type β-Ga_2O_3 crystals.[15–18] However, fabricating p-type crystals of β-Ga_2O_3 has proven to be very challenging, which limits its potential applications. Recently, considerable attention has been directed towards identifying suitable p-type dopants for β-Ga_2O_3. Despite extensive efforts, p-type single crystals of β-Ga_2O_3 have not yet been successfully produced. Various metal acceptors, such as Zn, Mg, and Ni, have been investigated as potential dopants in β-Ga_2O_3, but the results suggested deep acceptor behaviors of the dopants. Among these dopants, Ni-doped β-Ga_2O_3 samples show promise for producing semi-insulating substrates for lateral power devices. Gustafson *et al.*[19] have grown a Ni-doped β-Ga_2O_3 crystal by the Czochralski method using an iridium crucible and radio frequency heating. As a result, the presence of Ir impurity is unavoidable. In fact, by using electron paramagnetic resonance and optical absorption, the presence of Ni and Ir substitution at gallium sites was reported by Gustafson

[a]*Department of Mathematics and Physics, Universitetet i Stavanger, Stavanger, Norway*
[b]*Engineering Research Group, Dong Nai Technology University, Bien Hoa City, Vietnam*
[c]*Faculty of Engineering, Dong Nai Technology University, Bien Hoa City, Vietnam*
[d]*College of Natural Sciences, Can Tho University, Can Tho City, Vietnam*
[e]*Faculty of Physics, School of Education, Can Tho University, Can Tho City, Vietnam*
[f]*Semiconductor Materials Division, Department of Physics, Chemistry and Biology, Linköping University, SE-581 83, Linköping, Sweden*
[g]*Faculty of Applied Sciences, HCMC University of Technology & Education, 01 Vo Van Ngan, Thu Duc, Ho Chi Minh City, Vietnam*
[h]*Laboratory for Computational Physics, Institute for Computational Science and Artificial Intelligence, Van Lang University, Ho Chi Minh City, Vietnam. E-mail: khanh.nguyenduy@vlu.edu.vn*
[i]*Faculty of Mechanical – Electrical and Computer Engineering, School of Technology, Van Lang University, Ho Chi Minh City, Vietnam*

et al.[19] The optical absorption peaks at 303 nm and 442 nm were assigned to Ni at the octahedral site. When irradiated at 275 nm, the concentration of Ni^{3+} increases and the Ir^{4+} concentration decreases. After increasing the temperature above 375 °C, the concentration of Ni^{3+} and Ir^{4+} is restored. In addition, the Ni acceptor level is reported at 1.4 eV above the VBM. In the report of Seyidov *et al.*[20] the acceptor level of Ni was reported at 1.9 eV and a deep donor level at 1.1 eV above the VBM, which was not reported by Gustafson *et al.*[19] In the case of unintentional doping with Ir, Ir_{Ga} was reported to be an n-type donor, the EPR study indicated nonmagnetic ($S = 0$) Ir^{3+}, while Ir^{4+} was reported as $S = 1/2$ in ref. 19 and 21. In ref. 22, Ir exhibited both double and single donor behaviors, whereas in the study by Zachinskis and co-workers,[23] only the single donor state of Ir at the Ga site was observed.

While standard density functional theory (DFT) and its modified versions, such as DFT + U and DFT + U + V, have played a significant role in understanding the electrical and optical properties of semiconductors.[24–27] They are not enough when applied to defects in wide band-gap materials.[28,29] In recent years, hybrid functionals have emerged as a promising alternative for studying wide band-gap semiconductors, particularly screened hybrids[30,31] with the HSE06 functional developed by Heyd, Scuseria, and Ernzerhof being especially notable[32,33] More recently, the optimized hybrid functional calculation method has demonstrated its advantages in studying defects in various wide-bandgap semiconductors, including GaN, $CuGaS_2$, and cubic-ZnS.[34–36] For β-Ga_2O_3, the optimized hybrid functional with parameters ($\alpha = 0.26$, $\mu = 0.00$) has already shown its advantages in reproducing and explaining experimental results both with intrinsic defects and,[13,37,38] with the substitution of metals at the Ga site.[39,40] The procedure for obtaining the optimized parameters that reproduce the gap-optimized, Koopmans' theorem-compliant hybrid functional for β-Ga_2O_3 has been discussed in the section III of ref. 37. Although, numerous studies have investigated Ni and Ir in β-Ga_2O_3, a comprehensive understanding of these two impurities considering various aspects such as formation energy, spin states, and the Fermi-level remains incomplete. In this research, the optimized hybrid functional will be employed to investigate Ni- and Ir-doped β-Ga_2O_3. In this paper, HSE(0.26,0.00) will be used to investigate Ni- and Ir-doped β-Ga_2O_3. By comparing our calculated results with previous experimental and simulation studies, this research aims to provide a complete understanding of Ni and Ir impurities in β-Ga_2O_3. This includes examining formation energies, the most favorable spin states of defects, and correlating Ni and Ir concentrations with EPR spectra, optical absorption, and predicting luminescence emission peaks associated with Ni and Ir substitution in β-Ga_2O_3.

2. Computational details

In this report, the gap-optimized, Koopmans' theorem-compliant hybrid functional HSE, with 26% Hartree–Fock exchange ($\alpha = 0.26$) and a conventional hybrid functional ($\mu = 0.00$), where exchange interactions are treated uniformly, was employed. Calculations were carried out using the Vienna *Ab initio* Simulation Package (VASP 5.4.4) along with the projector augmented wave (PAW) method.[41–43] The semi-core d electrons of gallium were treated as part of the valence shell. A plane-wave basis set cutoff was set at 420 eV, with a kinetic energy cutoff for augmentation charges at 840 eV. In this study, Ni and Ir are doped into the 3D bulk structure of β-Ga_2O_3. A 160-atom supercell, constructed as a 1 × 4 × 2 expansion of the base-centered monoclinic unit cell, was used for defect calculations. The supercell has dimensions of approximately 12.2 Å × 9.1 Å × 11.6 Å, and the lattice parameters adopted for this work are $a = 12.25$ Å, $b = 3.04$ Å, $c = 5.82$ Å, and $\beta = 103.8°$.[37] The self-consistent electronic energy was converged to 10^{-4} eV, with ion relaxation continuing until forces on each ion were reduced to below 0.02 eV $Å^{-1}$. Calculations employed the Γ-approximation for Brillouin zone sampling, proven to be convergent within 0.1 eV for this supercell size in the previous work.[44] To mitigate artificial interactions between repeated images of charged defects, the charge correction method from ref. 45 and a high-frequency dielectric constant of $\varepsilon_\infty = 3.55$ (ref. 2) have been used in our calculations.

3. Results and discussion

In β-Ga_2O_3, there are two nonequivalent gallium sites: one with tetrahedral coordination and one with octahedral coordination. The formation energies of nickel and iridium incorporation on the 2 inequivalent gallium sites in different charge states are shown in Fig. 1, as a function of the Fermi-level position between the calculated valence band maximum (VBM) and the conduction band minimum (CBM), using the following expression:

$$E^{\mathrm{f}}[\mathrm{X}^{\mathrm{q}}] = E_{\mathrm{tot}}[\mathrm{X}^{\mathrm{q}}] - E_{\mathrm{tot}}[\mathrm{Ga_2O_3}] - \sum_i n_i\mu_i + \mathrm{q}E_{\mathrm{F}} + E^{\mathrm{q}}_{\mathrm{corr}} \quad (1)$$

where $E_{\mathrm{tot}}[\mathrm{X}^{\mathrm{q}}]$ and $E_{\mathrm{tot}}[\mathrm{Ga_2O_3}]$ represent the total energies of the structures containing the substitution X (Ni and Ir in the current research) at charge state q and the pristine β-Ga_2O_3 supercell, respectively. n_i indicates the number of atoms added to ($n_i > 0$) or removed from ($n_i < 0$) the pristine supercell to form the defect. $E^{\mathrm{q}}_{\mathrm{corr}}$ is the correction for the finite-size supercell approach as described in the computational details. μ_i represents the chemical potential of the atoms in the reservoir corresponding to the crystal growth conditions. The E_F is the Fermi-level position between the VBM and CBM. The chemical potential of μ_{Ni} is bounded by the formation of $NiGa_2O_4$ in the O-rich limits ($\Delta H[NiGa_2O_4] = -13.79$ eV, the calculated heat of formation of $NiGa_2O_4$) and Ga_3Ni_2 in the Ga-rich limit ($\Delta H[Ga_3Ni_2] = -2.24$ eV). While in the case of iridium the chemical potential μ_{Ir} is set by Ga_9Ir_2 in the Ga-rich condition ($\Delta H[Ga_9Ir_2] = -4.95$ eV) and IrO_2 in the O-rich condition ($\Delta[IrO_2] = -2.92$ eV).

In Fig. 1, the red lines represent the charge transition levels of Ni incorporating on Ga sites (Ni_{Ga}). The results indicate that Ni substitution at the octahedral site (Ni_{Ga_2}) is energetically preferred over the tetrahedral site (Ni_{Ga_1}) across all charge states. This result is in good agreement with previous

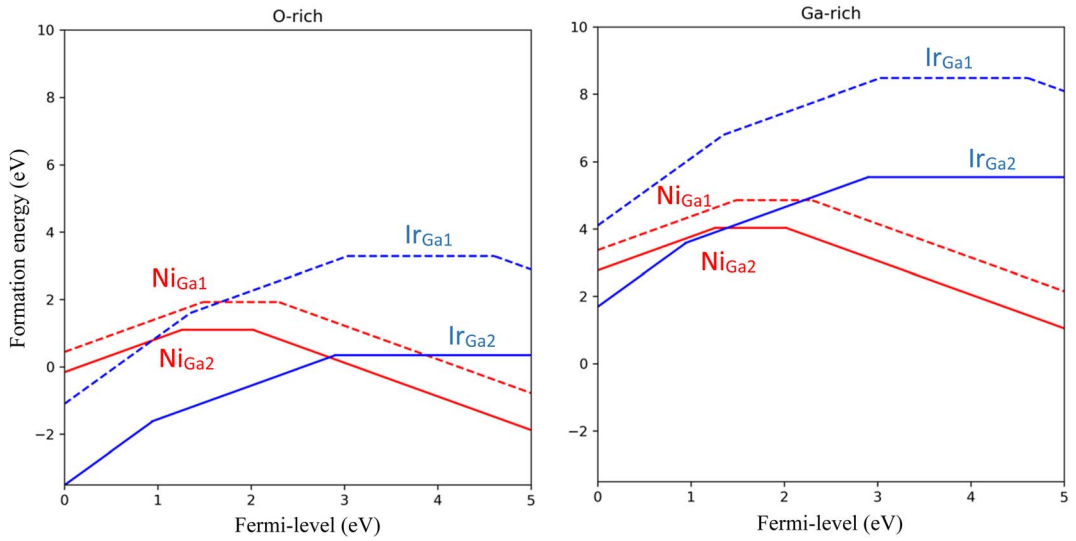

Fig. 1 Formation energy (eV) of Ni_{Ga} and Ir_{Ga} under as a function of the Fermi-level position.

studies.[19,20] Ni_{Ga} show deep acceptor behaviors with low formation energies for both sites under n-type conditions. The calculated acceptor levels (0/−1) are 2.02 eV and 2.30 eV above the VBM for Ni_{Ga_2} and Ni_{Ga_1}, respectively. Our calculated results are higher in energy compared to the theoretical charge transition levels in the work of Seyidov *et al.*[20] For the donor states (0/+1), the transition levels are found at 1.26 eV and 1.48 eV above the VBM for Ni_{Ga_2} and Ni_{Ga_1}, respectively. The differences in the charge transitions levels in our calculations and those in ref. 20 are likely from the choice of using the parameters in hybrid functional and dielectric constant used in charge correction.

In this study, it was also found that substitutional Ni at both Ga sites is preferred in the spin-triplet states in the acceptor state, and the spin-singlet state is more favorable in the neutral charge state. This finding aligns well with the research of Seyidov and co-workers.[20] In the donor state, Ni_{Ga_2} has the lowest formation energy in the singlet spin state, while Ni_{Ga_1} is stable in the spin-triplet state compared to the non-magnetic singlet spin state which is 0.65 eV higher in formation energy. The spin-triplet state of Ni_{Ga_1} in the donor charge state is likely caused by the difference in ionic radii between tetrahedral Ga^{3+} (47 pm) and Ni^{2+} (69 pm). The larger substitutional Ni ion at the tetrahedral Ga site causes a distortion that likely triggers the Jahn–Teller effect which removes the degeneracy and lowers the system's energy, thus achieving a more stable configuration in the triplet spin state. The singlet spin state of Ni_{Ga_2} in the +1 charge state aligns with the findings of ref. 20, but the donor state of Ni_{Ga_1} site was reported to be stable in spin-quartet state in that report.[20]

Fig. 1 also displays the formation energy of Ir incorporating at Ga sites (Ir_{Ga}), by the blue lines. Similar to Ni substitution, Ir substitution at the octahedral Ga site is energetically preferred compared to the tetrahedral Ga site due to the ionic radius of Ir (68 pm). The octahedral Ga ion (62 pm) provides more space to accommodate the larger ionic radius of Ir compared to the tetrahedral sites. Ir substitution at the Ga_2 site (Ir_{Ga_2}) minimizes lattice strain and leads to more stable dopant incorporation. Ir_{Ga_2} shows donor behavior, with charge transition levels at 0.94 eV (+2/+1) and 2.9 eV (+1/0). For substitution at the tetrahedral site, the donor states have charge transition levels at 1.35 eV and 3.03 eV for (+2/+1) and (+1/0), respectively. It was also found that Ir_{Ga_1} has an acceptor state with a charge transition (0/−1) occurring in the band gap at 4.61 eV above the VBM, the compensated acceptor level of Ir_{Ga_1} was also reported by Ritter *et al.*[22] Our calculated results for Ir_{Ga} charge transition levels and formation energies are in good agreement at the (+2/+1) transition, but show deeper energy at (+1/0) compared to other studies.[22,23]

It should be noted that while Ritter and coworkers[22] reported all charge states, the authors did not specify the spin state of the substitution. On the other hand, Zachinskis *et al.*[23]

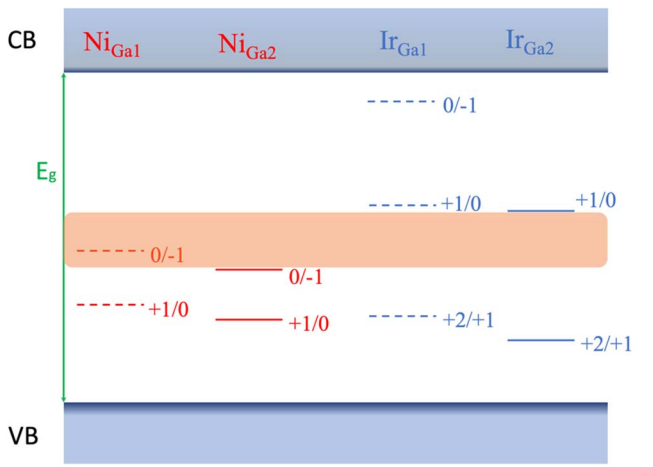

Fig. 2 The schematic band diagram illustrates the defect-level energies for Ni_{Ga} and Ir_{Ga} defects. The shaded orange row indicates the estimated Fermi-energy range.

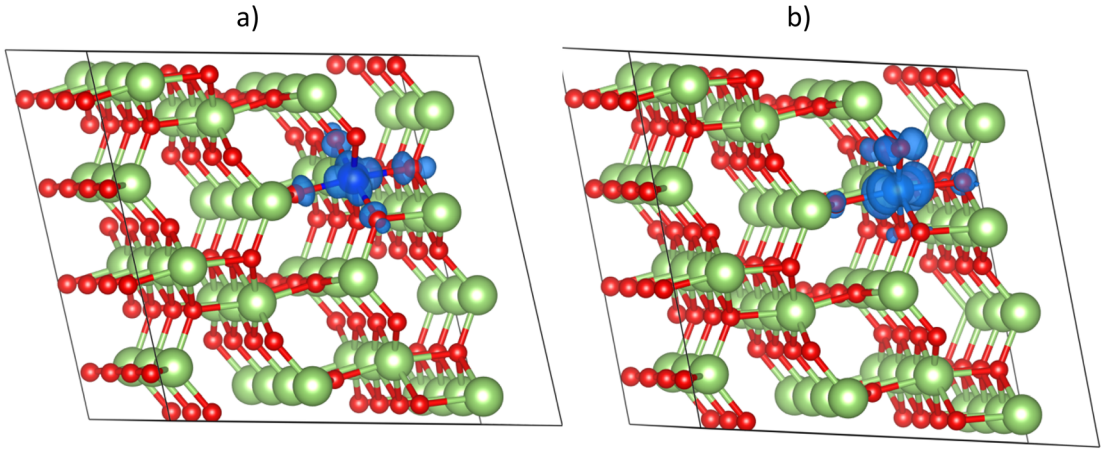

Fig. 3 Diagram of (a) Ni and (b) Ir substitution at Ga_2 site. The green and red balls represent Ga, O, respectively. The blue lobes show the localization of electron (a) $Ni_{Ga_2}^{0}$ and (b) $Ir_{Ga_2}^{1+}$ in the spin-singlet state.

demonstrated that the high spin state $S = 4/2$ has the lowest formation energy for Ir_{Ga2} in the neutral charge state, and $S = 3/2$ is energetically favorable for Ir_{Ga_1} in the singly donor state. However, no information on the double donor state was provided. In our calculation, for the neutral charge state, Ir_{Ga_2} adopts the singlet spin state, while Ir_{Ga_1} has the lowest formation energy in the spin-triplet state, which is 0.25 eV lower than that of the singlet spin state. It is due to the distortion caused by the larger Ir dopant at the Ga_1 site and the Jahn–Teller effect, as discussed above with Ni_{Ga_1} in the donor charge state. In the singly donor states, Ir_{Ga} at both substitution sites is most stable in the $S = 1/2$ spin state. The most favorable state for Ir_{Ga_2} in the doublet spin state is in good agreement with the observation of Ir^{4+} in EPR measurements.[19,21]

Experimental studies have shown that Ir is often present in β-Ga_2O_3 as an unintentional dopant, especially in Ni-doped β-Ga_2O_3 crystals grown by the Czochralski method.[22,46,47] EPR measurements by Gustafson *et al.*[19] have identified the signals of Ni and Ir substitution at Ga sites and their concentration correlation. Specifically, when a Ni-doped sample is irradiated with 275 nm light, the concentration of Ni^{3+} ions increase, while the concentration of Ir^{4+} ions decrease. The concentration of Ni^{2+} can be restored by heating above 375 °C.[19] The above EPR results can be explained as follows: when the sample is doped with an acceptor dopant like Ni, the correlation between unintentional n-type dopants (such as Si and H) and Ni pins the Fermi-level around the middle of the band gap, similar Fermi-level range was also reported in ref. 20. If one considers the Fermi-level as in the shaded orange row of Fig. 2, Ni_{Ga_2} and Ir_{Ga_2} are energetically favorable in the −1 (Ni^{2+}) and +1 (Ir^{4+}) charge states, respectively. When the sample is irradiated with 275 nm light, electrons are excited to the conduction band, leading to Ni_{Ga_2} and Ir_{Ga_2} are identified at 0 (Ni^{3+}) and +2 (Ir^{5+}) charge states. Thus, the EPR measurement shows an increase of Ni^{3+} ion and a decrease in Ir^{4+} ion concentration after irradiation. When the sample is heated, electrons recombine with holes, that witness the restoration of Ni^{2+} and Ir^{4+} concentrations.

Fig. 3 illustrates the localization of electrons at the spin state $S = 1/2$ of $Ni_{Ga_2}^{0}$ and $Ir_{Ga_2}^{1+}$, corresponding to Ni^{3+} and Ir^{4+}, as addressed in the experimental studies.[19] The wave functions of

Table 1 Charge transition levels with respect to the calculated VBM and CBM (eV), in comparison with values in recent studies in both experimental and HSE calculations

Defects	Transition levels	Experimental transition	Recent HSE calculations	This work HSE(0.00,0.26)	Optical absorption	Recent HSE calculations	This work HSE(0.00,0.26)
Ni_{Ga_2}	+1/0	X	VBM +1.09 (ref. 20)	VBM +1.26	CBM −4.09 (ref. 19)	CBM −3.8 (ref. 20)	CBM −4.25
	0/−1	VBM +2.0 (ref. 20) VBM +1.4 (ref. 19)	VBM +1.88 (ref. 20)	VBM +2.02	CBM −2.81 (ref. 19)	CBM −3.16 (ref. 20)	CBM −2.56
Ir_{Ga_2}	+2/+1	CBM −2.2 (ref. 46)	VBM +1.01 (ref. 22)	VBM +0.94	CBM −2.9, −3.5, −4.4 (ref. 48)	X	CBM −4.54
	+1/0		CBM −2.25 (ref. 22) (VBM +2.6) CBM −2.58 (ref. 23) (VBM +2.15)	CBM −2.1 (VBM +2.9)	CBM −2.8 (ref. 22)	CBM −2.99 (ref. 23)	CBM −2.92

electrons in this spin state are not only localized at the substitutional site but also at several oxygen sites around the substitutional sites. This spread of wave function localization explains the broad EPR lines of Ni^{3+} and Ir^{4+} ions in the experimental observation.[19,21] In the analysis of Ni-doped β-Ga_2O_3 crystals, Gustafson *et al.*[19] also found broad optical absorption bands at 442 nm (2.81 eV) and 303 nm (4.09 eV), which were attributed to Ni substitutions. Experimental data of optical absorption peaks are often interpreted as vertical electron transitions from the defect to the CBM.[29,37] In our calculations, the vertical charge transitions of Ni at (+1/0) and (0/−1) are 2.56 eV and 4.25 eV below the CBM, respectively. This is in good agreement with the experimental results in ref. 19. In the case of Ir_{Ga_2}, the vertical transition levels are calculated at 2.92 eV and 4.54 eV for the neutral and +1 charge states, respectively. The vertical transition of the neutral charge state is in line with the study by Ritter *et al.*,[46] which reports an absorption at 2.8 eV. Further details on the comparison of the optical absorption and the calculated vertical transition energies for Ni and Ir substitutions are provided in Table 1.

We also predicted the emission energy, which corresponds to the emitted wavelength from the recombination of an electron with a hole. The recombination was calculated considering a limited-size supercell, resulting in an accuracy of 100 meV for the photoluminescence energy. The difference between an electron in a shallow donor state and a conduction band electron bound by the trapped hole has not been considered. Therefore, an electron is considered to be at the CBM. The equilibrium geometry of the bound exciton was relaxed under the constraint of the orbital occupations, and the spin multiplicity was kept constant during the entire process. As explained above, the correlation between unintentional dopants and Ni acceptors places the Fermi-level in the middle of the gap. Therefore, under irradiation, the electron of donor Ni_{Ga_2} is excited to the CBM and then recombines with the hole. In the case of Ir_{Ga_2} this process occurs in the +1 charge state. The calculated recombination energy between a trapped hole at Ni^{2+} and an electron at the CBM was found to be 2.23 eV, while for Ir^{4+}, it is 2.55 eV. The luminescence of Ir_{Ga_2} has yet to be confirmed, but it is likely due to the inadvertent Ir impurity.

4. Conclusion

This study shows a detailed theoretical investigation of Ni and Ir dopants in β-Ga_2O_3 using the optimized hybrid functional HSE(0.26,0.00), which closely agree with experimental results. The calculations results reveal that both Ni and Ir exhibit a strong preference for substitution at the octahedral gallium site. Ni dopant demonstrates dual donor and acceptor behaviors at charge transition levels (+1/0) 1.0 eV and (0/−1) 2.24 eV above the VBM, Ir impurity shows donor behaviors with charge transition levels (+2/+1) at 1.04 eV and (+1/0) at 3.15 eV above the VBM. These results align well with recent experimental measurements, including the correlation between Ni and Ir ion concentrations observed in electron paramagnetic resonance studies. Moreover, the calculated vertical transition levels for Ni_{Ga_2} (2.56 eV and 4.25 eV below the CBM) and Ir_{Ga_2} (2.91 eV and 4.62 eV below the CBM) correspond closely with experimental optical absorption peaks. This comprehensive analysis advances the understanding of Ni- and Ir-doped β-Ga_2O_3 and underscores their potential applications in optoelectronic devices, particularly in high-resistivity and semi-insulating substrates.

Data availability

The data that supports the findings of this study are available within the article.

Author contributions

Quoc-Duy Ho: conceptualization, investigation, data curation, methodology, formal analysis, visualization, writing – original draft. K. Dien Vo, Nguyen Thanh Tien, Huynh Anh Huy, and Duc-Quang Hoang: investigation, data curation, formal analysis, visualization, writing – editing. Duy Khanh Nguyen: supervision, investigation, data curation, validation, formal analysis, manuscript review and editing.

Conflicts of interest

The authors declare that they have no known competing financial interests or personal relationships that could have appeared to influence the work reported in this paper.

Acknowledgements

Duy Khanh Nguyen acknowledges the supports of Van Lang University (VLU), Ho Chi Minh City, Vietnam.

References

1 M. Orita, H. Ohta, M. Hirano and H. Hosono, *Appl. Phys. Lett.*, 2000, **77**, 4166.
2 J. Furthmüller and F. Bechstedt, *Phys. Rev. B*, 2016, **93**, 115204.
3 S. J. Pearton, J. Yang, P. H. I. V. Cary, F. Ren, J. Kim, M. J. Tadjer and M. A. Mastro, *Appl. Phys. Rev.*, 2018, **5**, 011301.
4 J. Zhang, J. Shi, D.-C. Qi, L. Chen and K. H. L. Zhang, *APL Mater.*, 2020, **8**, 020906.
5 J. Zhu, Z. Xu, S. Ha, D. Li, K. Zhang, H. Zhang and J. Feng, *Materials*, 2022, **15**, 7339.
6 A. Afzal, *J. Mater.*, 2019, **5**, 542.
7 M. M. Afandi, S. Jeong and J. Kim, *Opt. Mater.*, 2023, **146**, 114613.
8 T. Minami, T. Shirai, T. Nakatani and T. Miyata, *Jpn. J. Appl. Phys.*, 2000, **39**, L524.
9 Q. Li, *et al.*, *Catal. Commun.*, 2019, **120**, 23.
10 Y. Hou, L. Wu, X. Wang, Z. Ding, Z. Li and X. Fu, *J. Catal.*, 2007, **250**, 12.
11 E. Filippo, M. Tepore, F. Baldassarre, T. Siciliano, G. Micocci, G. Quarta, L. Calcagnile and A. Tepore, *Appl. Surf. Sci.*, 2015, **338**, 69.

12 J. B. Varley, J. R. Weber, A. Janotti and C. G. Van de Walle, *Appl. Phys. Lett.*, 2010, **97**, 142106.
13 N. T. Son, Q. D. Ho, K. Goto, H. Abe, T. Ohshima, B. Monemar, Y. Kumagai, T. Frauenheim and P. Deák, *Appl. Phys. Lett.*, 2020, **117**, 032101.
14 P. D. C. King, I. McKenzie and T. D. Veal, *Appl. Phys. Lett.*, 2010, **96**, 062110.
15 S. C. Siah, *et al.*, *Appl. Phys. Lett.*, 2015, **107**, 252103.
16 A. Mauze, Y. Zhang, T. Itoh, E. Ahmadi and J. S. Speck, *Appl. Phys. Lett.*, 2020, **117**, 222102.
17 F. Alema, G. Seryogin, A. Osinsky and A. Osinsky, *APL Mater.*, 2021, **9**, 091102.
18 W. Zhou, C. Xia, Q. Sai and H. Zhang, *Appl. Phys. Lett.*, 2017, **111**, 242103.
19 T. D. Gustafson, N. C. Giles, B. C. Holloway, J. Jesenovec, B. L. Dutton, J. S. McCloy, M. D. McCluskey and L. E. Halliburton, *J. Appl. Phys.*, 2022, **132**, 185705.
20 P. Seyidov, J. B. Varley, J.-X. Shen, Z. Galazka, T.-S. Chou, A. Popp, M. Albrecht, K. Irmscher and A. Fiedler, *J. Appl. Phys.*, 2023, **134**, 205701.
21 C. A. Lenyk, *et al.*, *J. Appl. Phys.*, 2019, **125**, 045703.
22 J. R. Ritter, J. Huso, P. T. Dickens, J. B. Varley, K. G. Lynn and M. D. McCluskey, *Appl. Phys. Lett.*, 2018, **113**, 052101.
23 A. Zachinskis, J. Grechenkov, E. Butanovs, A. Platonenko, S. Piskunov, A. I. Popov, J. Purans and D. Bocharov, *Sci. Rep.*, 2023, **13**, 8522.
24 Y. Z. Abdullahi, R. Caglayan, A. Mogulkoc, Y. Mogulkoc and F. Ersan, *JPhys Mater.*, 2023, **6**, 025003.
25 A. Akyildiz, I. Ilgaz Aysan, Y. Z. Abdullahi, B. Akgenc Hanedar, Z. Demir Vatansever and F. Ersan, *Phys. Chem. Chem. Phys.*, 2024, **26**, 26566.
26 Y. Z. Abdullahi, *Comput. Condens. Matter*, 2021, **29**, e00614.
27 Y. Z. Abdullahi and F. Ersan, *RSC Adv.*, 2023, **13**, 3290.
28 W. R. L. Lambrecht, *Phys. Status Solidi B*, 2011, **248**, 1547.
29 C. Freysoldt, B. Grabowski, T. Hickel, J. Neugebauer, G. Kresse, A. Janotti and C. G. Van de Walle, *Rev. Mod. Phys.*, 2014, **86**, 253.
30 S. J. Clark and J. Robertson, *Phys. Rev. B: Condens. Matter Mater. Phys.*, 2010, **82**, 085208.
31 X. Zheng, A. J. Cohen, P. Mori-Sánchez, X. Hu and W. Yang, *Phys. Rev. Lett.*, 2011, **107**, 026403.
32 J. Heyd, G. E. Scuseria and M. Ernzerhof, *J. Chem. Phys.*, 2003, **118**, 8207.
33 A. V. Krukau, O. A. Vydrov, A. F. Izmaylov and G. E. Scuseria, *J. Chem. Phys.*, 2006, **125**, 224106.
34 P. Deák, M. Lorke, B. Aradi and T. Frauenheim, *Phys. Rev. B*, 2019, **99**, 085206.
35 M. Han, Z. Zeng, T. Frauenheim and P. Deák, *Phys. Rev. B*, 2017, **96**, 165204.
36 Q. Duy Ho and M. Castillo, *Comput. Mater. Sci.*, 2023, **216**, 111827.
37 P. Deák, Q. Duy Ho, F. Seemann, B. Aradi, M. Lorke and T. Frauenheim, *Phys. Rev. B*, 2017, **95**, 075208.
38 Q. D. Ho, T. Frauenheim and P. Deák, *Phys. Rev. B*, 2018, **97**, 115163.
39 Q. D. Ho, D. K. Nguyen and H. A. Huy, *Comput. Condens. Matter*, 2022, **32**, e00727.
40 Q. D. Ho, T. Frauenheim and P. Deák, *J. Appl. Phys.*, 2018, **124**, 145702.
41 G. Kresse and D. Joubert, *Phys. Rev. B: Condens. Matter Mater. Phys.*, 1999, **59**, 1758.
42 G. Kresse and J. Furthmüller, *Phys. Rev. B: Condens. Matter Mater. Phys.*, 1996, **54**, 11169.
43 G. Kresse and J. Hafner, *Phys. Rev. B: Condens. Matter Mater. Phys.*, 1994, **49**, 14251.
44 P. Deák, Q. D. Ho, F. Seemann, B. Aradi, M. Lorke and T. Frauenheim, *Phys. Rev. B*, 2017, **95**, 075208.
45 C. Freysoldt, J. Neugebauer and C. G. Van de Walle, *Phys. Rev. Lett.*, 2009, **102**, 016402.
46 J. R. Ritter, K. G. Lynn and M. D. McCluskey, *J. Appl. Phys.*, 2019, **126**, 225705.
47 Z. Galazka, *et al.*, *ECS J. Solid State Sci. Technol.*, 2017, **6**, Q3007.
48 J. Jesenovec, J. Varley, S. E. Karcher and J. S. McCloy, *J. Appl. Phys.*, 2021, **129**, 225702.